Geologica Acta, Vol.11, Nº 2, June 2013, 231-244
DOI: 10.1344/105.000001838
Available online at www.geologica-acta.com

geologica acta

Post-depositional processes of elemental enrichment inside dark nodular masses of an ancient aeolian dune from A Coruña, Northwest Spain

M.J. TRINDADE[1,4] **M.I. PRUDÊNCIO**[1,4] **J. SANJURJO-SÁNCHEZ**[2] **J.R. VIDAL ROMANÍ**[2]
T. FERRAZ[3] **D. FERNÁNDEZ MOSQUERRA**[2] **M.I. DIAS**[1,4]

[1] **Instituto Tecnológico e Nuclear, Instituto Superior Técnico, Universidade Técnica de Lisboa**
EN10, 2686-953 Sacavém, Portugal
Trinidade E-mail: mjtrindade@ctn.ist.utl.pt Prudêncio E-mail: iprudenc@ctn.ist.utl.pt Dias E-mail: isadias@ctn.ist.utl.pt

[2] **Instituto Universitario de Xeoloxía, Campus de Elviña, Universidade da Coruña**
A Coruña, España
Sanjurjo-Sánchez E-mail: jsanjurjo@udc.es Vidal Romaní E-mail: xemoncho@udc.es
Fernández-Mosquera E-mail: xemos@udc.es

[3] **Instituto Nacional de Engenharia, Tecnologia e Inovação**
Estrada do Paço do Lumiar 22, 1649-38 Lisboa, Portugal
Ferraz E-mail: teresa.ferraz@lneg.pt

[4] **GeoBioTec Research Centre, Universidade de Aveiro**
Campus Universitário de Santiago, 3810-193 Aveiro, Portugal

ABSTRACT

This paper focuses on a residual ancient aeolian climbing dune from Punta Penaboa (A Coruña, Northwest Spain) showing evidence of post-depositional weathering, particularly the presence of dark brown nodular masses. The partitioning of trace elements between nodular masses and host sand during post-depositional weathering of the dune is investigated in this work, with the main objective of studying the elemental enrichment patterns in the dark masses. Data of the concentrations of chemical elements were obtained by instrumental neutron activation analysis (INAA) and complemented by mineralogical and microchemical studies, using X-ray powder diffraction (XRD) and scanning electron microscopy (SEM) / energy dispersive X-ray spectrometry (EDS). The dune was dated by optically stimulated luminescence (OSL) , yielding an age of 300ka B.P.. The dark nodular masses preserved the dune sand structure, without defined concentric layers, suggesting an early stage of formation. They consist mainly of quartz grains cemented by clay materials enriched in the majority of the elements studied, especially in Mn, Co, Ba, Sb, Ce, Tb, Th, As, Zr and Hf. The post-depositional transformations of the dune were most likely influenced by migration of chemical compounds from the surrounding slope deposits and granitic rocks, as well as microbial activity that promoted metals concentration in the solutions percolating through the pore network of the dune. Seasonal changes in the redox potential were required to produce the accumulation of Mn and other trace elements in the dune pore network and to promote the fractionation between Ce^{4+} and trivalent rare earth elements that was observed in the geochemical patterns.

KEYWORDS | **Dune. Manganese. Oxidation. Trace elements. Weathering.**

INTRODUCTION

The littoral of A Coruña province in Galicia (NW Spain) is a high energy irregular coast composed of beaches separated by headlands, embayed beach barriers, and deep marine embayments (Alonso and Pagés, 2007). The intense development of aeolian processes is revealed by the presence of several aeolian coastal dune systems along the coastline, much of them are remains of the ones that were alternately formed and destroyed during the Quaternary glacioeustatic oscillations.

The aeolian deposits of the NW Spanish coast occur in two distinct facies: i) type one corresponds to active and inactive recent dunes that predominate in the South, in the lower coast sections. They are associated with the last sea level rise episode, with an age comprised between 5 ka B.P. and the actuality (Devoy *et al.*, 1996; López Cancelo, 2004). It consists of various kinds of dunes (barchan, parabolic, among others) that are more or less stabilized by vegetation; ii) type two corresponds to inactive fossil aeolian deposits, which predominate in the North, in places where the coast is steeper. It consists of cemented sand wedges, commonly intercalated in solifluction deposits, located at different highs above sea level (Vidal Romaní, 1986; Flor, 1992; Granja and Carvalho, 1992). These deposits correspond to ancient climbing dunes, whose age has been determined by the co-authors of this paper from the Instituto Universitario de Xeoloxía, being the present work an initial contribution to this matter.

The morphological analysis of the dune systems and information on the recent climatic conditions, characterized by high degree of humidity in a temperate maritime climate heavily moderated by the Atlantic Ocean, suggests that the dunes were formed in different conditions than the present day ones: i) lower sea level to allow larger source area of sediments feeding the dunes by the wind action; ii) more arid climate with lower temperatures and predominating steppe vegetation, which difficult dune stabilization and iii) stronger wind regime with enough intensity and continuity to promote greater energy for their displacement and movement. In fact, the formation of Galicia dune systems disconnected from actual beaches is frequently positioned in a regressive period inside the Holocene transgressive tendency, characterized by lower temperatures than the current ones (Santos *et al.*, 1993; Mosquera Santé, 2000; Vidal Romaní *et al.*, 2000; Blanco Chao *et al.*, 2003; López Cancelo, 2004).

The dune sections exposed in Hercynian granitic cliffs from the A Coruña coast were initially discovered and described by Vidal Romaní (1974). They are most likely the response to prolonged aeolian erosion of the coast during almost 80ka in which persisted regressive marine conditions (Roucoux *et al.*, 2006). The dune sections have been interpreted as remains of a climbing dune, formed due to unidirectional winds that piled up the beach sand against the rock face cliff encroaching on its summit and afterward, the rise of sea level produced disconnection of the dune from their source area, becoming an inactive deposit. Later, the cliffs were degraded by periglacial processes during the Glacial period, with the altered mantle moving downslope by solifluction and translational landsliding (Alonso and Pagés, 2007). During these processes, the Interglacial highstand levels were covered by periglacial sediments, consisting mainly of debris flows and breccias (Alonso and Pagés, 2000), and remained protected, enabling the preservation of the aeolian episodes as well as the raised beaches (conglomeratic layers) that are common in the North Spain coast (Nieto and Vidal Romaní, 1989).

Post-depositional processes such as compaction, bioturbation, pedogenesis, cementation and weathering are responsible for the modification of primary textures and mineralogical characteristics of dune sands. The chemical elements can be mobilized and deposited elsewhere into secondary phases or adsorbed onto mineral phases. The mobilization is driven by a variety of mechanisms (precipitation-dissolution, sorption-desorption, reduction-oxidation), both pH and redox potential being considered the most critical parameters controlling the distribution of metals (Cao *et al.*, 2001).

The dune section under study shows as particular post-depositional feature the presence of dark nodular masses produced by the enrichment of manganese and other elements with affinity to Mn-oxyhydroxides. The presence of Fe-Mn nodules in different continental environments, especially in soils and laterites have been reported and studied extensively (Sanz *et al.*, 1996; Coelho and Vidal-Torrado, 2000; Palumbo *et al.*, 2001; Dowding and Fey, 2007; Neaman *et al.*, 2008). However, little is known about the formation of Mn nodules in dune sands under the temperate maritime climatic conditions that characterize A Coruña coast.

The present work aims at enhancing the knowledge of the geochemical and mineralogical modifications in dune sands as a consequence of post-depositional weathering by comparing the composition of the dark nodular masses rich in manganese with the surrounding host sand. In particular, the mobility of trace elements, including the Rare Earth Elements (REE), and the enrichment geochemical patterns in the dark nodular masses are investigated.

MATERIALS

The aeolian dune section studied is located in Punta Penaboa (Monte de San Pedro), in the coast of A Coruña province (Galicia, NW Spain). Two outcrops of the same

deposit were identified (Vidal Romaní, 1974; Gutiérrez Becker *et al.*, 2004), which are situated above and below the coastal promenade constructed between San Roque de Afuera and O Portiño (Fig. 1). The aeolian deposit is placed about 20m above present sea level in a zone of granite and leucogranite substrate. The outcrop studied, located further west, exhibits maximum dimensions of about 50m by 6m.

The dune consists of light brown cemented sand, with evidence of some post-depositional features, especially the presence of reddish layers of iron-oxides and dark brown masses resembling nodules with sub-spherical shape and millimetric size (Fig. 2). These are not compact concretions with concentric structure. Instead they correspond to weak nodule development, and therefore they will be referred to as dark nodular masses. The nodular masses consist of sand enriched in certain elements like Mn, black coloring the sand.

The aeolian deposit is affected by bioturbation exerted by the colonization of plants, especially due to rooting of Utex europaeus, which has its roots deep and robust (Vidal Romaní, 1974).

The local stratigraphy, from base to top, consists of: i) substrate of granitic rocks; ii) a conglomeratic layer with 2.5m of maximum thickness, formed by large blocks of quartz and granite cemented by kaolinite, which has been interpreted as a palaeobeach level (Flor, 1992; Alonso and Pagés, 2007); iii) a solifluction deposit (slope deposit) consisting of angular fragments, generally of granitic rocks, in a brown silty sand matrix rich in organic matter; iv) a residual aeolian dune located at about 20m above sea level of approximately 8m thickness and 300m in length (Gutiérrez Becker *et al.*, 2004). The sequence ends with another solifluction deposit, forming a discordant erosive contact with the aeolian deposit.

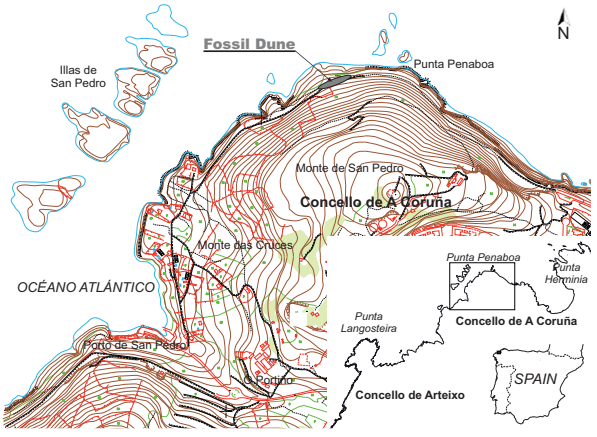

FIGURE 1 | Location of the studied dune at Punta Penaboa (A Coruña, Spain). Adapted from the cartographic maps of the Concello de A Coruña (sheets 021-62,63,64,72,73,81), scale 1:5000, from the Consellería de Política Territorial Obras Públicas e Vivenda, Dirección Xeral de Urbanismo, Xunta de Galicia.

FIGURE 2 | Aspect of the dark nodular masses in the Penaboa dune.

Twelve samples, including altered granite, solifluction deposits and dune sand, were collected along a vertical profile (Fig. 3). The solifluction deposit samples were sieved to separate the broken fragments (>2mm fraction) from sand, and both fractions were analyzed. Four samples of dune rich in dark nodular masses (samples PPB1 to PPB4, from base to top) were collected at different heights of the aeolian deposit. Each dune sample was then separated in one subsample corresponding to the host sand (PPBx.1) and another subsample corresponding to the dark masses (PPBx.2). The conglomeratic paleobeach level fed by cliff erosion of granitic rocks was previously studied (Vidal Romaní, 1974) and not analyzed in this work.

Two samples (05/009-Penaboa 1 and 05/010-Penaboa 2) of the ancient aeolian dune were collected for luminescence dating by OSL. Sample 05/009-Penaboa 1 comes from the dune section studied in this work, whereas sample 05/010-Penaboa 2 was collected in another section of the same dune located approximately 50m east of sample 05/009-Penaboa 1. Samples were collected by hammering steel tubes (30cm long and 10cm diameter) on the dune sections, sealing them with opaque black plastic. The transported tubes to the laboratory were opened under adequate illumination conditions (red light), rejecting the first 10cm of sediment of each extreme of the tubes. Coarse quartz grains of 180-250μm size were separated by sieving and extracted by chemical digestion with HCl, H_2O_2 and HF to eliminate carbonates, organic matter

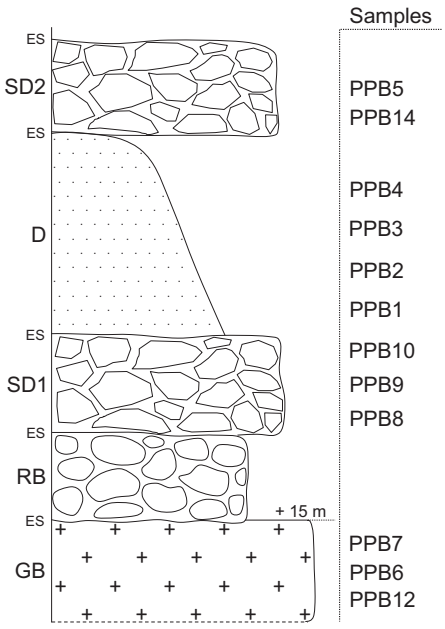

FIGURE 3 | Schematic stratigraphic column and samples collected at Punta Penaboa. GB: granitic basement; RB: residual beach; SD: slope deposit; D: dune; ES: erosive surface.

and feldspars, respectively. Very pure quartz (no Infrared Stimulated Luminescence emission (IRSL)) was obtained and grains were mounted on Al discs using silicone spray.

METHODS

All samples were pulverized in agate mortar and prepared to the mineralogical and chemical analysis by X-ray diffraction (XRD) and instrumental neutron activation analysis (INAA), respectively. These techniques were complemented with observations in scanning electron microscopy (SEM) / energy dispersive X-ray spectrometry (EDS). Dune age estimates were obtained by optically stimulated luminescence (OSL).

X-ray Diffraction (XRD)

The identification of crystalline phases of finely pulverized samples was obtained with a Philips X'Pert Pro diffractometer, using CuKα radiation, scanning of 1º per minute and operating at 45kV and 40mA. The <63μm fraction (obtained by wet sieving) of dune samples was also studied as it helps the identification of accessory minerals that are generally obscured by the abundance of quartz.

Semi-quantitative estimates of mineral abundances were achieved by measuring the areas of diagnostic reflections and weighting by empirical reflection powers, according to criteria recommended by Schultz (1964) and Thorez (1976).

Instrumental Neutron Activation Analysis (INAA)

INAA was used to determine the chemical composition of samples due to its multi-elemental capability, high precision and accuracy, and low detection limit. Samples and standards (GSD-9 and GSS-1 from the Institute of Geophysical and Geochemical Prospecting) were irradiated together in the pneumatic system of the Portuguese Research Reactor (PRR) for 1.5min (short irradiation) and in the core grid of PRR for 6h (long irradiation), at a thermal flux of 3.96×10^{12}ncm^{-2} s^{-1}, ϕ_{th}/ϕ_{fast}= 29.77, ϕ_{ep}/ϕ_{th}= 1.03%. The gamma spectra were recorded by high-resolution Ge detectors. For details concerning the measurement and processing of the gamma spectra see Gouveia and Prudêncio (2000) and Dias and Prudêncio (2007).

Scanning Electron Microscopy/Energy Dispersive X-ray Spectrometry (SEM-EDS)

Sample fragments were dried at room temperature and coated with gold by a Fine Coat ion sputter JFC-1100 from JEOL, using 10mA for 5min, corresponding to a coating thickness of 400-500Aº, which depends on the orientation of samples. The observations were made with a Philips XL30 FEG microscope at Laboratório de Caracterização de Materiais (INETI, Portugal). Chemical maps of dune samples rich in dark nodular masses were obtained in cross-section surfaces after embedded in epoxy resin, cutting and polishing with sandpaper and successive diamond pastes of 6μm, 3μm and 1μm diameter. Thereafter, they were cleaned by immersion in alcohol in an ultrasound bath. Polished cross-sections coated with gold were observed with a JEOL JSM 6400 Scanning Electron Microscope at 16keV and EDS analyses were carried out with an Oxford Inca Energy 200 EDS equipment, at Instituto Universitario de Xeoloxía (University of Coruña, Spain).

Optically Stimulated Luminescence (OSL)

OSL essentially measures the last time a mineral grain was exposed to sunlight (*i.e.* when the mineral grain experienced burial). Buried grains are exposed to ionizing radiation (estimated as the dose rate) from the decay of radioactive elements and their daughter products, as well as cosmic rays (Aitken, 1998). The mineral grains serve as a natural dosimeter, and the accumulated dose is estimated as equivalent dose (D_e) by exposure to light in a luminescence reader. Such light stimulates luminescence emission by mineral grains (OSL). The age (time since burial) is calculated by dividing D_e by the dose rate of ionizing radiation within the sediment. The most used mineral for OSL is quartz, because it is ubiquitous, resistant to weathering and its luminescence signal is stable over geological timescales. Aeolian sediments are the most suitable sediments for OSL dating (Aitken, 1998).

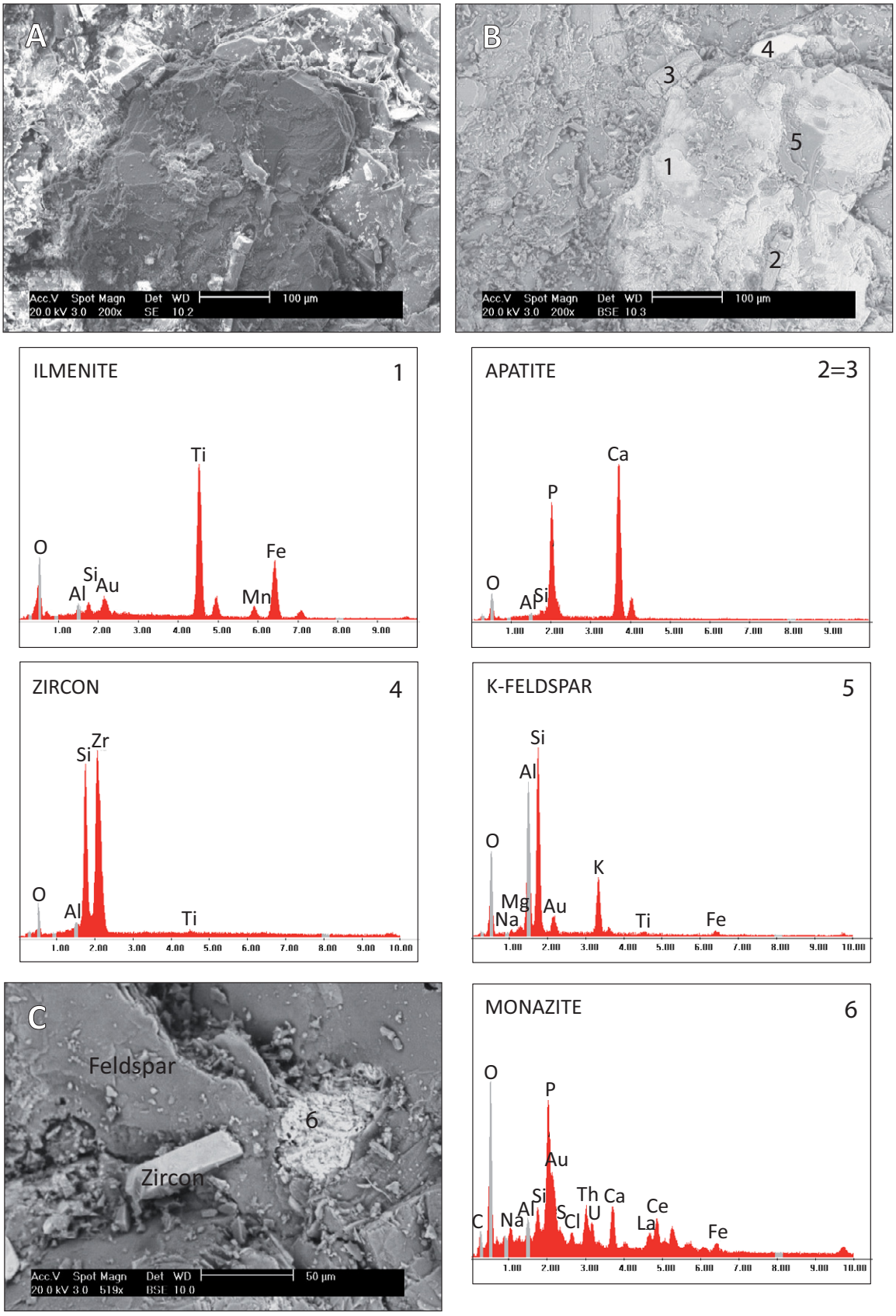

FIGURE 4 | A) Secondary and B and C) backscattered electron SEM-EDS images for the less altered granite sample (PPB12), standing out ilmenite, apatite, zircon, monazite and K-feldspar crystals.

OSL ages were stimulated using blue light and the Single Aliquot Regeneration (SAR) procedure (Murray and Wintle, 2003). SAR measurements were performed at 125ºC, during 40s after 260ºC preheat for 10s (preheat chosen after performing preheat tests for both samples). The first 0.8 seconds (5 channels) were used to measure OSL signals and the last 4 seconds for background (25 channels). A Risø TL/OSL-DA-15 reader model was used for all quartz luminescence measurements, using an internal $^{90}Sr/^{90}Y$ source that provides 0.120±0.003Gy/s. Equivalent doses were calculated by interpolation from Analyst software integration data (1% systematic error

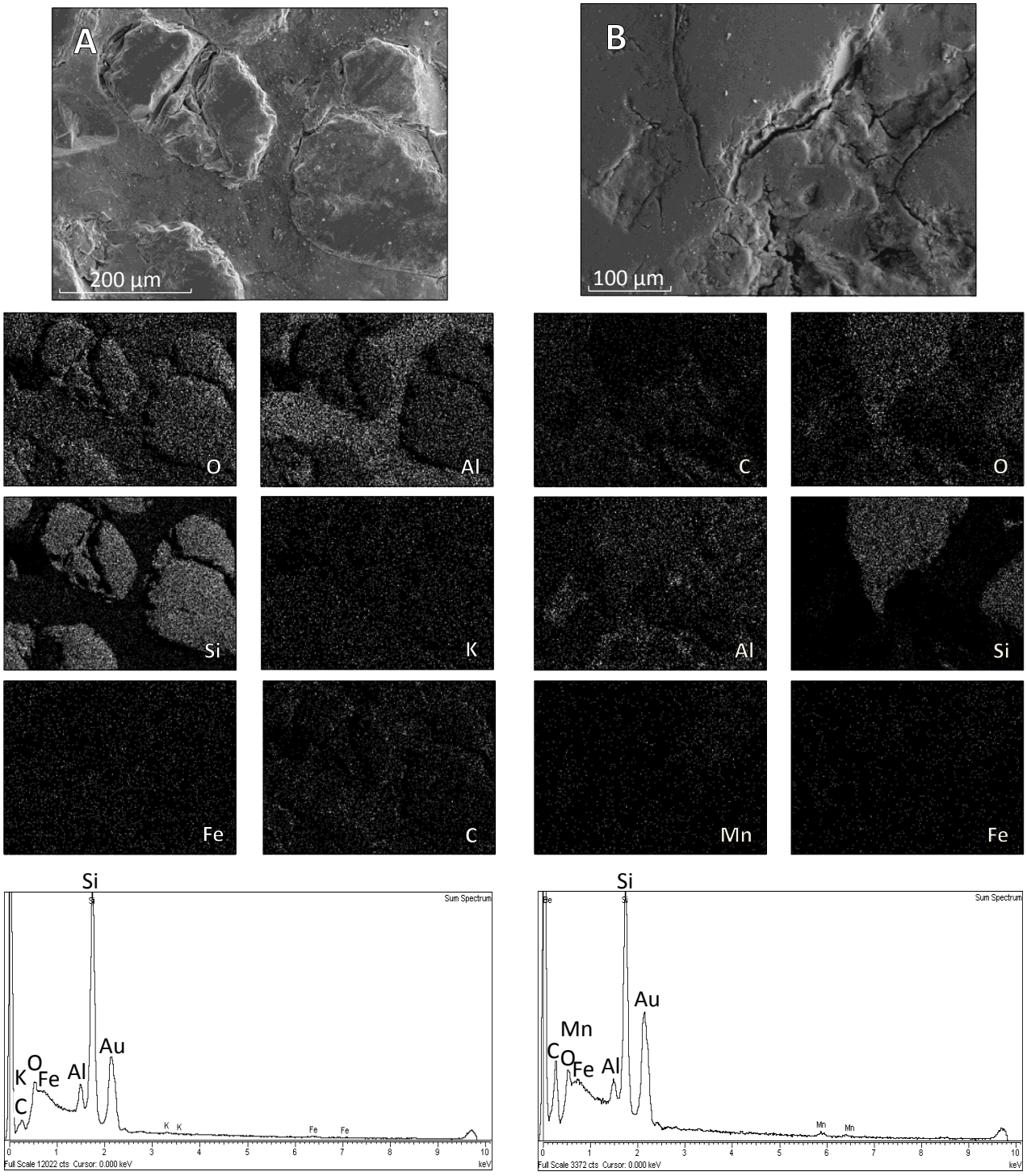

FIGURE 5 | Cross-section X-ray maps by SEM-EDS of nodular masses from A) sample PPB2 and B) sample PPB4.

incorporated). The equivalent doses used to calculate the ages were determined after observation of histograms and radial-plots build with the D_e obtained from aliquots.

The internal zone of the samples was also used to determine the concentrations of radioactive elements and disintegration products of ^{238}U, ^{232}Th, ^{235}U and ^{40}K radioactive series by high resolution gamma spectrometry, using a Ge Canberra XtRa GX6020 detector. Results were then used to obtain the proportion of ionizing energy adsorbed per year by quartz grains (annual dose or dose rate). Conversion factors of radionuclide activities to determine the annual dose were taken from Adamiec and Aitken (1998). Water content and saturation were estimated, and attenuation was considered to calculate the dose rate. The contribution of cosmic rays in annual dose is included in annual dose calculation in accordance to Prescott and Hutton (1995).

RESULTS

Mineralogy

Altered granites consist mainly of quartz, K-feldspar (Kfs) and plagioclase (Pl), with Kfs/Pl ratios above unit (Electronic Appendix Table I avaliable at www.geologica-acta.com). Minor amounts of mica and rare kaolinite are also present. The <2mm fraction of slope deposits is mainly composed by quartz and feldspars, with Kfs/Pl ratios below the unit, and traces of mica and kaolinite, whereas the angular fragments consist mainly of quartz and plagioclase, with minor amounts of K-feldspar and mica.

The dune samples have high amounts of quartz (96-99%) and display Na-rich plagioclase, K-feldspar and phyllosilicates (mainly kaolinite) as accessory phases. The mineralogical composition of the dune indicates that the dune sand was originated from granitic rocks. In order to search for more mineralogical post-depositional evidence in dune sands, besides the presence of kaolinite and illite, the mineralogy of the <63μm fraction was also studied. The analysis of this fraction enabled identification of gibbsite in all dune samples, indicating high degree of weathering after deposition of sands under humid conditions. The kaolinite-gibbsite association is frequent in NW Portugal and Galicia as a result of intense weathering of granite rocks (Sequeira Braga *et al.*, 2002).

The X-ray diffraction patterns of finely ground nodular material, from the whole rock and <63μm fraction, show they are mineralogically similar to the host sand, not allowing the identification of manganese minerals.

SEM-EDS

SEM observations in the less altered granite sample (PPB12) enable to recognize others accessory minerals beyond those identified by XRD, namely a Ti-Fe rich phase (probably ilmenite), apatite and zircon associated with

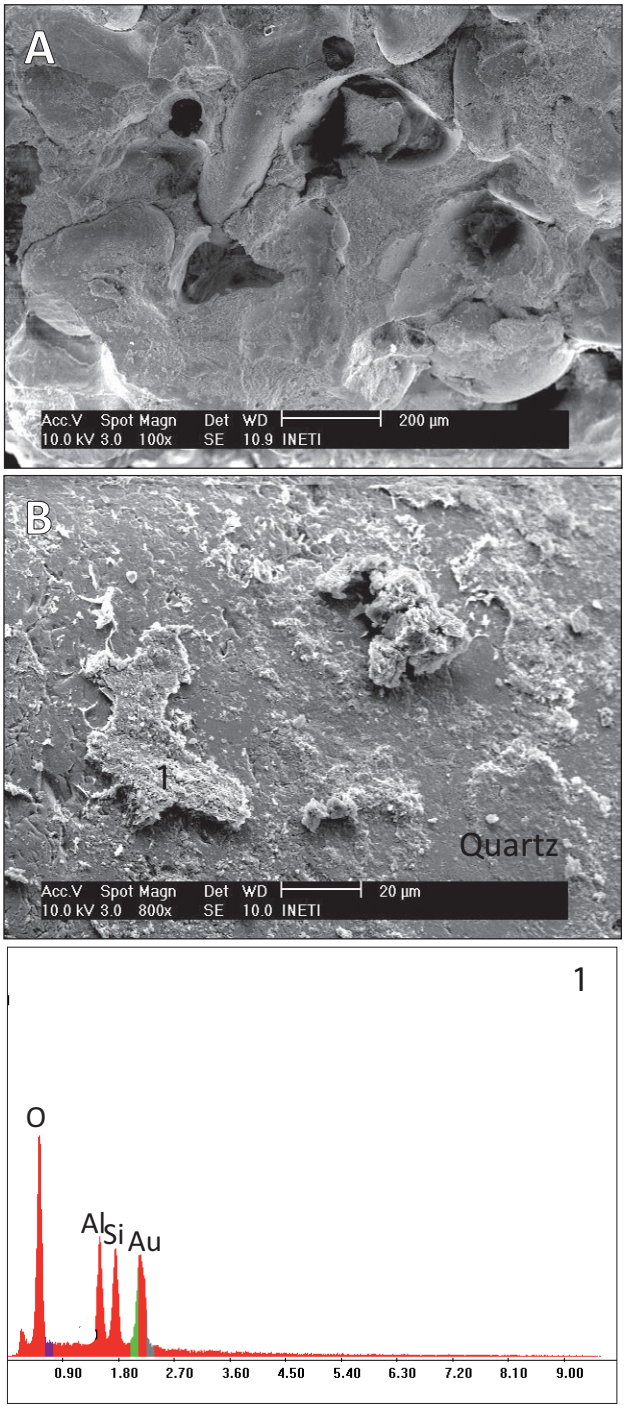

FIGURE 6 | Secondary electron SEM-EDS images of the A) host sand and B) kaolinite coating on quartz grains (sample PPB4.1).

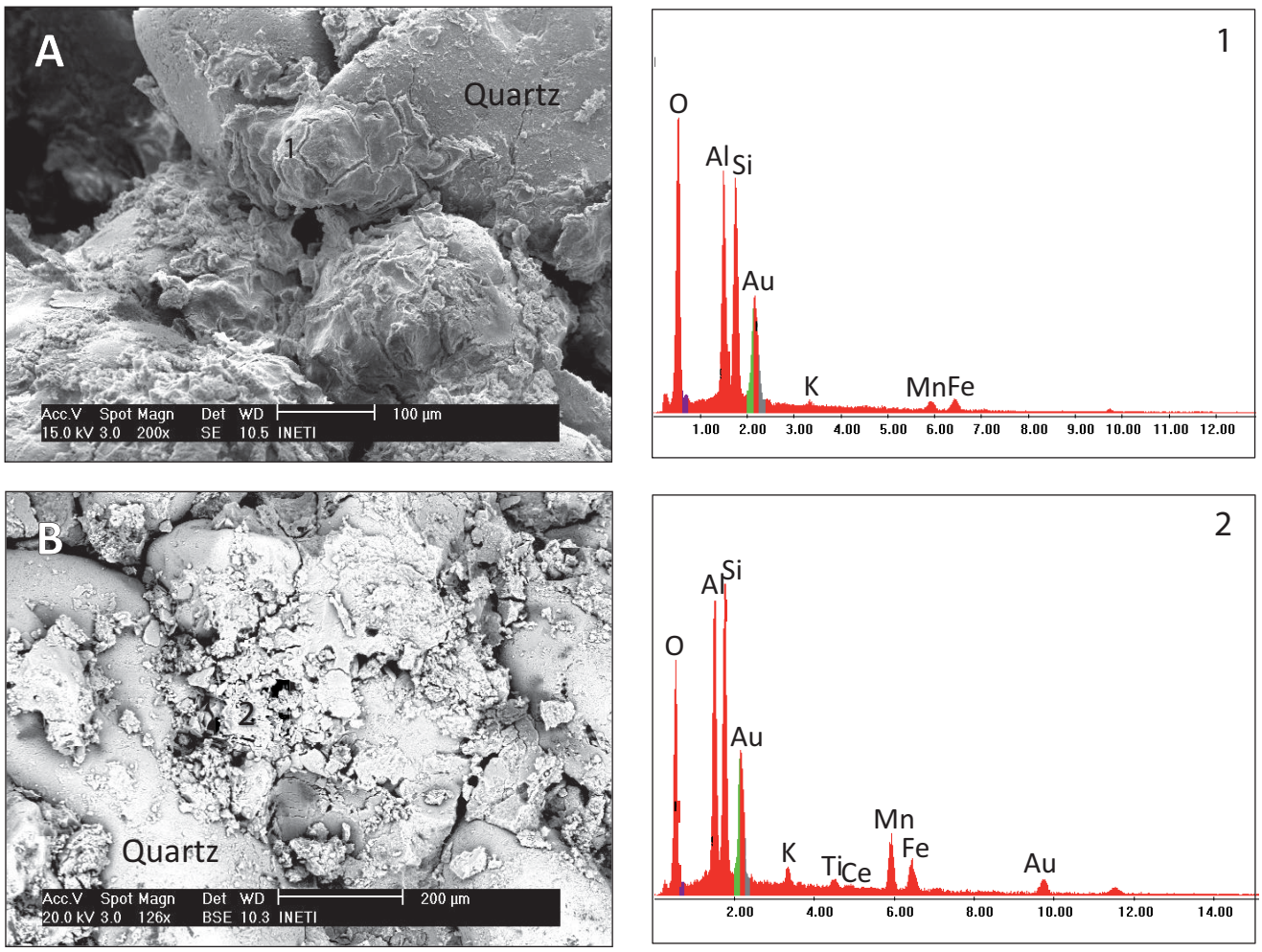

FIGURE 7 | Secondary electron SEM-EDS image showing a clay coating with Mn and Fe on quartz grains in A) sample PPB2.2, and backscattered SEM-EDS image showing a clay coating with Mn, Fe and Ce on quartz grains in B) sample PPB4.2.

K-feldspar. Various grains of monazite, containing Ce, La, Th and U, as well as a Fe-rich phase with traces of Mn over the feldspar were also found (Fig. 4).

Electron microprobe X-ray maps (Fig. 5) of the surface cross-section of two dune samples (PPB2.2 and PPB4.2) show that dark nodular masses are mainly composed by rounded Si-O (quartz) grains embedded in a matrix with high Al content, which is also found over quartz grains in lower amounts. Traces of C, Fe, K and Mn may dot the studied surfaces.

SEM observations of unpolished surfaces (Figs. 6, 7) show similar features for the dark nodular sand and the host sand. Both consist of quartz grains cemented by clay, yet differing slightly in the chemical composition of the grains coating, which consists only of O, Al and Si (gibbsite and/or kaolinite) in the host sand (Fig. 6), but it has Mn and Fe, and sometimes Ce, added in the case of the dark nodular masses (Fig. 7). The accumulation of these elements along with the aluminum coating supports the idea of post-depositional modification of the aeolian deposit.

Geochemistry

The concentrations of major and trace elements in the studied samples are given in Tables II and III. The average elemental concentrations display a similar distribution in granites and in sand fraction of slope deposits, but with slightly lower concentrations of several elements in the last one. This depletion (mainly in Th, Co, Sc, U and rare REEs) is even more accentuated in the broken fragments of slope deposits. The dune has lower concentrations of most elements relative to granites, except in Mn, Cr and Co (Fig. 8).

The dune samples have similar chemical composition (Fig. 9), except sample (PPB4) collected on top of the profile that has higher contents of most elements, especially Mn and Co, suggesting it has higher quantity of dark nodular masses than the other samples.

The host sand dune shows Fe_2O_3T/MnO ratios in the range of 35.5-77.9, whereas much lower ratios are observed in the nodular masses, varying from 0.94 to

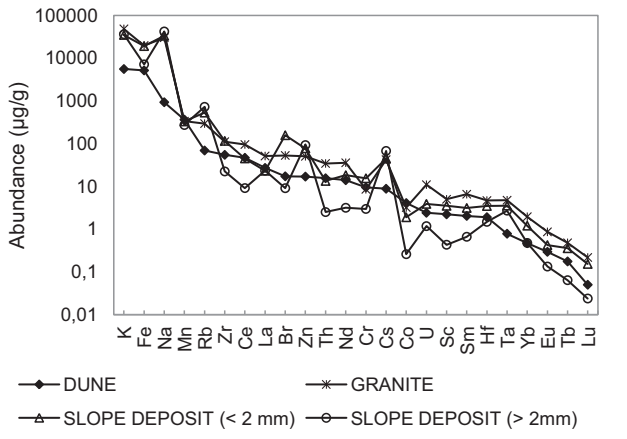

FIGURE 8 | Average chemical concentrations (in order of decreasing abundance relative to average dune content) for dunes, granitic rocks and slope deposits.

3.42. Therefore, the manganese enrichment in the nodular masses is not accompanied by similar iron enrichment in Fe-Mn oxyhydroxides.

The post-depositional elemental mobility is assessed by comparing the nodular masses and the host sand of each dune sample. The element enrichment factor (EF) was calculated according to Ahrens *et al.* (1967) as element concentration in nodule / element concentration in surrounding sand. The EF average values show that dark nodular masses are richer in the majority of the elements studied, especially in Mn, Co, Ba, Sb and Ce, than the host sand (Electronic Appendix Table IV). The enrichment pattern is similar in the various dune samples with only small differences that are related to the degree of enrichment of some elements, such as Mn and Ce. The concentrations of Na, K, Rb, Cs and Cr tend to decrease slightly in the dark nodular masses, suggesting that they were transported in solution to out of the weathered dune. The chondrite normalized rare earth element (REE) patterns (Fig. 10) are characteristic of sedimentary rocks, showing fractionation between light REE (LREE) and heavy REE (HREE) and a negative europium anomaly - log[3Eu*/(2Sm*+Tb*)], the superscript "*" implies the concentration normalized to chondrite. Comparing the nodular masses with the host sand of each dune sample it is clear that the first ones are enriched in all REEs. The LREE-HREE fractionation degree and the europium anomaly do not vary consistently between nodules and host sand (Electronic Appendix Table V), but different degree of positive cerium anomaly - log[3Ce*/(2La*+Nd*)] - in the nodule subsamples is clear. It is also evident an increase of the Ce anomaly in nodular masses from top (PPB4.2) to base (PPB1.2) of the profile, accompanying the enrichment of Mn downward (Electronic Appendix Table IV), as shows the Mn-Ce positive correlation (r = 0.81). Weaker correlations were observed between Mn and Zn, Sb and Th.

OSL dating

Results of the several measurements used for dating the two dune samples by OSL are shown in Electronic Appendix Table VI.

Results of the gamma spectrometry show weak disequilibrium in the radioactive series of ^{238}U for both samples, indicating that after deposition of sediments the geochemical system did not behave as a closed system. This may have important influence in the annual dose calculation. Radioactive disequilibrium suggests that the illuviation suffered by the ancient aeolian sands caused some migration of dissolved species, also allowing a mixture of grains is possible, which is feasibly explained by the own sedimentary dynamics of a climbing dune. The calculated deviation of the dose rate estimation and the final age should consider such disequilibrium.

The dose response OSL growth curves were fitted with a saturating exponential plus linear response. For most aliquots the observed natural doses lie onto the high dose linear region of the OSL growth curve. The onset of saturation for the saturating exponential is described by the parameter D_0 (natural dose). It has been suggested that reliable OSL dating is feasible up to two times the D_0 value (Murray and Wintle, 2006).

The accepted aliquots (showing negligible recuperation and thermal transfer) show Gaussian distribution when histograms are plotted. Also, radial plots show most aliquots grouped around a central value within the 2θ deviation interval (Fig. 11). Thus, the fitted central D_e (observed from radial-plots) has been considered to calculate the OSL age. It is noteworthy that the arithmetic mean D_e calculated from the aliquots fits both the weighted mean and the D_e calculated by the Central Age Model (CAM) (Galbraith and Laslett, 1993; Galbraith *et al.*,

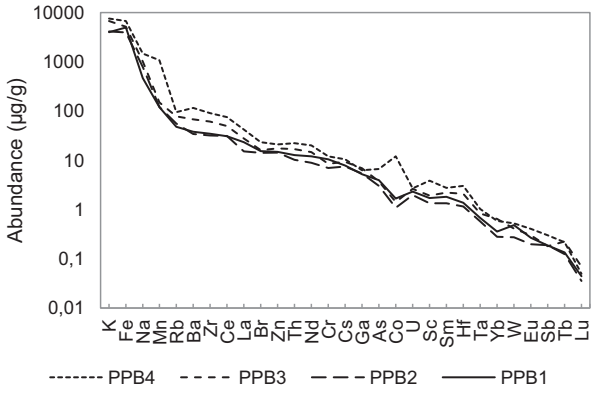

FIGURE 9 | Elemental abundance in the four dune samples studied (in order of decreasing abundance relative to average dune concentration).

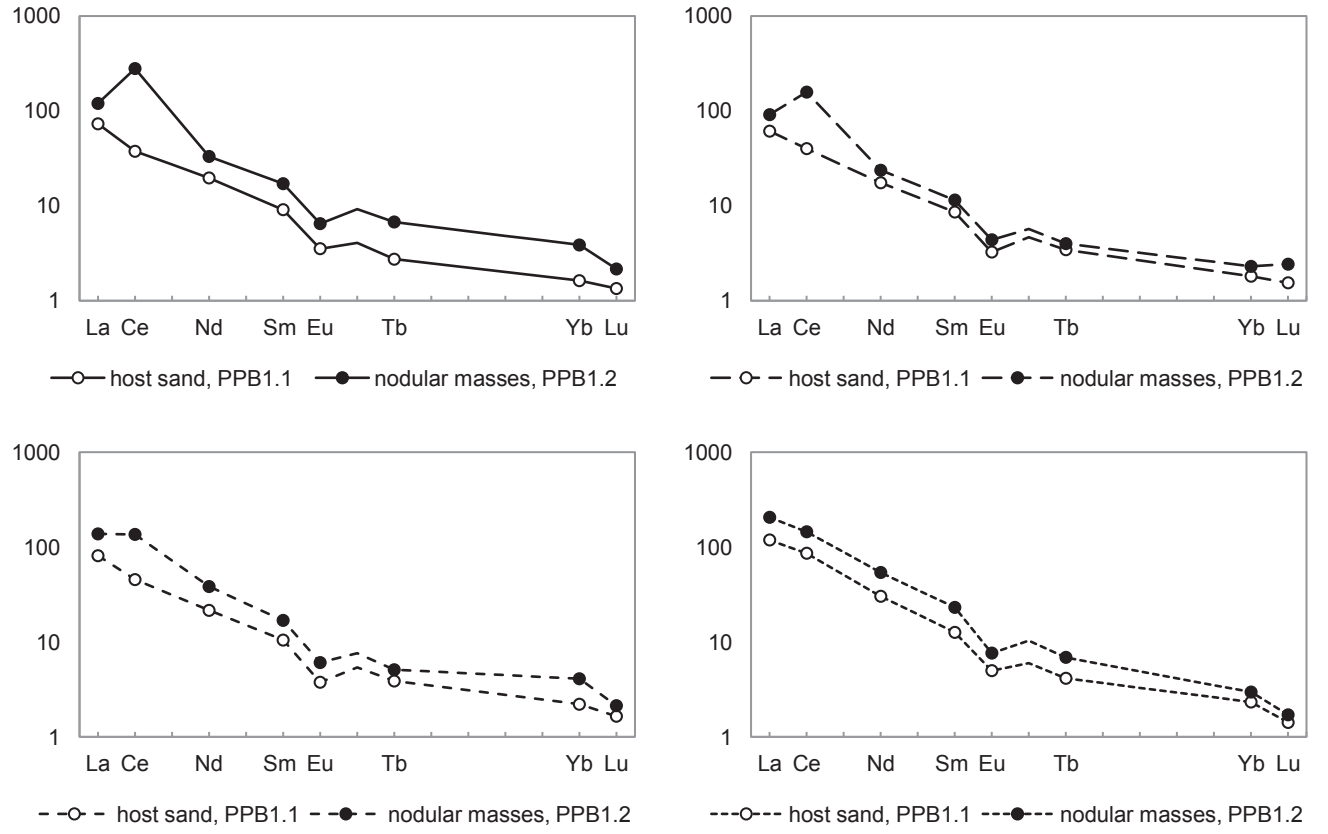

FIGURE 10 | Chondrite-normalized REEs patterns of dune samples (values of Anders & Grevesse, 1989, multiplied by the factor 1.36, according to Korotev, 1996).

1999) in accordance with the protocol established by Bailey and Arnold (2006). Nonetheless, CAM provides very short deviation due to the low overdispersion of aliquots (below 17% and 10% for 05/009-Penaboa 1 and 05/010-Penaboa 2, respectively). CAM assumes that the grains received a dose range around a central D_e, which is consistent with geological and dosimetrical data. However, due to the high doses and possible grain mixing expected for climbing dunes, a 2θ confidence interval has been considered to calculate the equivalent dose (the CAM would provide deviations of 6% and 4% for 05/009-Penaboa 1 and 05/010-Penaboa 2, respectively). The validity of the analysis adopted to determine the age is corroborated by the internal consistency between both studied samples, which have quite similar age (292 ± 51 ka B.P. in sample 05/009-Penaboa 1 and 304 ± 49ka B.P. in sample 05/010-Penaboa 2) as it is logical for samples from the same sedimentary unit. This internal stratigraphic consistency is a powerful indicator of the potential validity of age estimates. The age obtained for the aeolian dune inserts it into the Middle Pleistocene, in an interglacial period.

OSL ages are consistent but show older ages than those commonly obtained by quartz OSL. This is probably due to two factors: i) the low dose rates obtained (~1Gy ka^{-1}) when compared with doses found in granite areas. This is undoubtedly due to the mineral composition of the dune with >96% of quartz. Ionizing radiation in sediments (Aitken, 1998) is due to the emission from ^{238}U, ^{232}Th, and ^{235}U and isotopes from their decay series present in zircons (almost absent) and the ^{40}K content in feldspars (very low) in the dune; ii) the sensitivity and the OSL growth curve response of quartz. Higher saturation dose can be observed in the quartz OSL growth curve for medium and slow OSL components than in the fast component (Wintle and Murray, 2006).

However, similar (~300Gy) or higher (than those obtained for our samples) equivalent doses (~426Gy) have been estimated for the fast component of blue-OSL of quartz grains (Watanuki *et al.*, 2005).

DISCUSSION

Dark mass formation

The dark brown nodular masses observed in the dune from Penaboa most likely resulted from precipitation of Mn-oxyhydroxides, as evidenced by the high Mn concentrations.

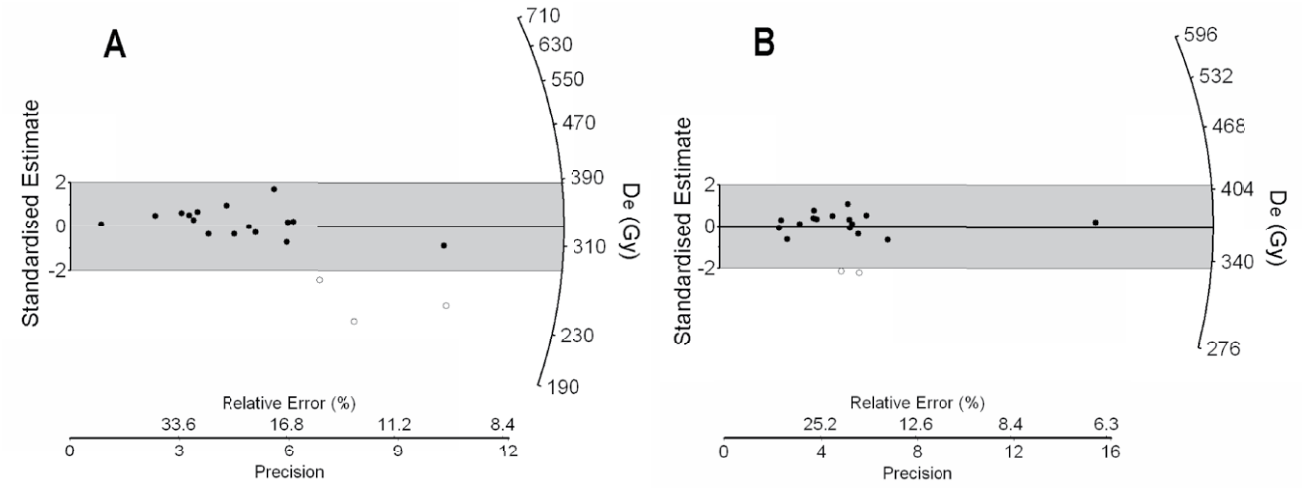

FIGURE 11 | Radial-plots of the OSL aliquots measured for A) 05/009-Penaboa 1 and B) 05/010-Penaboa 2.

Manganese oxyhydroxides are a common product of terrestrial weathering processes (Potter and Rossman, 1979; Roy, 2006) and occur in diverse environments. Nevertheless, the XRD mineralogical identification of the manganese minerals was not viable, probably due to the thinly particulate and disordered nature of the manganese forms and the presence of silicate phases as major components that may mask the peaks of Mn minerals (Gallaher *et al.*, 1973; Potter and Rossman, 1979). This suggests that the Eh-pH conditions were inadequate to the complete oxidation of Mn and formation of crystalline minerals or time to crystallize and development was not enough.

Manganese may originate from circulating water through surrounding bedrocks, containing minor amounts of Mn, or may result from diverse species of Mn-oxidizing bacteria (Hill, 1982; López-González *et al.*, 2006; Marín Arroyo *et al.*, 2008). As the rocks near the dune are not especially enriched in Mn (see Electronic Appendix Table II), the accumulation of this element in nodular masses within the dune can hardly be explained solely by percolation of Mn enriched waters resulting from weathering of background rocks. The influence of microbial activity, associated to decomposition of organic matter, in the formation of Mn rich nodular masses is advanced as a plausible hypothesis. However, further investigation is required to confirm it. In fact, several studies refer to the role of microorganisms, responsible for organic matter decomposition, in the formation of metal-organic complexes in a reducing environment, which are much more soluble and mobile than metallic ions themselves (Hill, 1982; Moffett, 1994; Marín Arroyo *et al.*, 2008). In such manner, they act as catalysts of oxidation-reduction reactions, enhancing metal activities and their effective solubilization and migration through the porous sediment. Although the abundance of organic matter in the stratigraphic units studied has not been determined, the field observations and previous works (Vidal Romaní, 1974; Gutiérrez Becker *et al.*, 2004) indicate the presence of organic activity (plant roots and bioturbation) in the dune. Also, some studies focusing periglacial coastal deposits in Northern Spain (Alonso and Pagés, 2000; Alonso and Pagés, 2007) show that the dark color of the solifluction deposits that cover the dune section derives from the high organic matter content, which might influence the dune composition.

The concentration of manganese in dark masses within the sediment pore network is likely linked to seasonal changes in the sediment redox potential and the degree of acidity/alkalinity of the environment (Sanz *et al.*, 1996; Zhang and

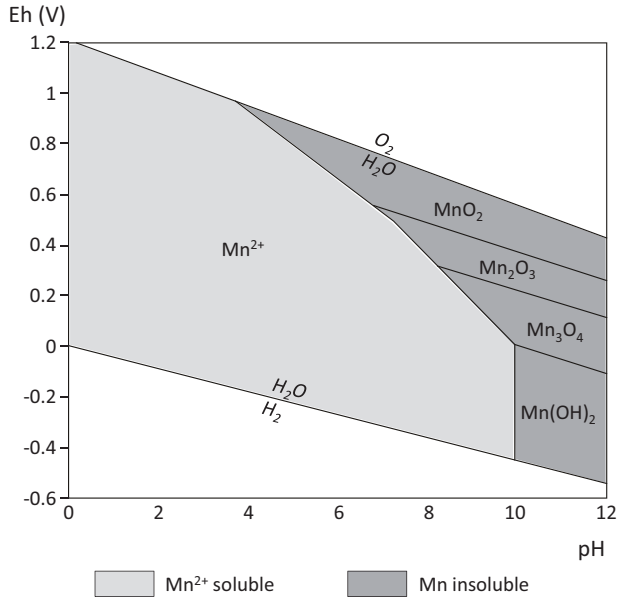

FIGURE 12 | Eh-pH stability diagram for manganese forms (adapted from Dorronsoro *et al.*, 2006).

Karathanasis, 1997). Considering the Eh-pH delimiting stability fields for Mn (Fig. 12) it is possible to provide an explanation of the different mechanisms involved in the genesis of manganese nodules, as suggested by Dorronsoro *et al.* (2006). Soluble manganese occurs in its reduced form (Mn^{2+}) and corresponds to the pH region below 10 and covers a large range of Eh (preferentially low values). An increase in pH and intensification of oxidizing conditions (associated with dry, well aerated sediments) would favor a change in manganese towards insoluble forms. On the contrary, in reducing conditions like in water saturated environments, soluble Mn^{2+} prevails. Therefore, precipitation of Mn oxides may be seen as a consequence of the solution dynamics. As superficial water passes through sediment it is charged with organic residues and acquires strong reducing capacity; it transports soluble Mn^{2+} until oxidizing conditions are found, then transforming manganese into insoluble forms and promoting its accumulation. Microorganisms probably acted as catalysts of the oxidation-reduction reactions.

Elemental associations

In this study, the Mn enrichment in nodular masses inside the dune is accompanied by high concentrations of most elements, mainly of Co, Ba, Sb and Ce, indicating fractionation among the REEs. Although REEs have similar chemical properties, low solubility, and in general are resistant to fractionation in supracrustal environments, fractionation can occur during weathering processes (Nesbitt, 1979; Braun *et al.*, 1990; Prudêncio *et al.*, 1993; Koppi *et al.*, 1996; Taunton *et al.*, 2000), and the weathered residual products are generally richer in LREE. The fractionation and mobilization of REEs in sediments depend upon pH and redox potential (Eh); the low pH and reducing conditions favor the REEs release from the sediments into solution (Cao *et al.*, 2001).

The higher abundance of Ce in the dark nodular masses in relation to the other REEs results from the Ce capacity of changing from the reduced state (Ce^{3+}) to the less soluble tetravalent state (Ce^{4+}) in oxidizing conditions, precipitating from solution as cerianite (CeO_2). Consequently, positive Ce anomalies may form in the chondrite-normalized REE patterns.

Weathering of primary minerals of granites, like mica and alkali feldspar, could be responsible for the supply of Ce^{3+} to the solution that percolates the sediment (Beauvais and Roquin, 1996). Moreover, SEM observations showed that the basement granites of Penaboa contain apatite and monazite, two host minerals for REEs, especially Ce. The alteration of these Ce-rich phases may also have contributed to enrich the solutions in Ce^{3+}.

The development of high-oxygen periodic conditions could have promoted the oxidation of Ce^{3+} to insoluble Ce^{4+} and its precipitation together with the relative immobile Mn^{3+}. The Ce enrichment observed in nodular masses and the significant correlation between Ce and Mn with increasing profile deep, suggest a relationship between Mn^{2+} and Ce^{3+} oxidation and a link among Ce distribution and the redox cycle of Mn (Palumbo *et al.*, 2001).

Other than Ce, elements like Co precipitated together with Mn-oxyhydroxides, probably as a result of Co^{2+} oxidation to Co^{3+}, as suggested by Burns (1976). This co-precipitation is possible due to the ability of Mn species to concentrate and control the distribution of certain metallic ions because of their high adsorption capacity for little hydrated cations (Mackenzie, 1989) motivated by strong electrical field in the Mn oxyhydroxides-solution interface (Murray and Dillard, 1979; Tan *et al.*, 2005). Additionally, microbial oxidation of Mn, due to the properties of the enzymes of the associated bacteria, favours co-precipitation under the same conditions (Moffett, 1994).

The reduced species of Mn and Co have similar stability fields (Coelho and Vidal-Torrado, 2000) requiring, in general, higher oxidation potentials to precipitate than those necessary to precipitate Ce and Fe (Mackenzie, 1989). The strong bound of Ce and other REEs, Co and U with Mn oxyhydroxides has been reported in several works (Taylor, 1968; Beauvis and Roquin, 1996; Koppi *et al.*, 1996).

CONCLUDING REMARKS

The formation of dark nodular masses in the middle Pleistocene aeolian dune resulted from post-depositional weathering, which led to loss of soluble substances, such as alkaline components (Na, K, Rb and Cs), and enrichment in insoluble substances, like hydrated aluminum and Mn oxyhydroxides that revealed to be good scavengers of various trace elements. However, the manganese minerals were not identified by XRD because they probably exist as low crystalline thin particles.

Apart from Mn, the dark nodular masses are especially enriched in Co, Ba, Sb and Ce relative to the surrounding host sand dune, with fairly similar enrichment pattern for the four nodular samples studied.

The most probable explanation for the formation of dark nodular masses within sand dune is by precipitation of Mn-rich solutions resulting from bacterial activity associated to decomposition of the organic matter coming from the slope deposits that involve the dune section and the soil level. The dry season induced oxygen transport into the pores of the sand forming micro-environments with oxidizing conditions that promoted oxidation of the reduced Mn existing in solution, followed by precipitation of Mn-oxyhydroxides, corresponding to a nucleus for nodules development. The pH and Eh are the main critical parameters controlling the distribution of Mn and associated metals, and their precipitation-dissolution cycles can be well explained by Eh-pH diagrams.

The increasing concentrations of Mn, Ce, Sb and other elements in the nodular masses located from the top to the base of dune profile (from PPB4 to PPB1), suggest increasing oxidizing conditions in direction to the base of the dune.

ACKNOWLEDGMENTS

Financial support for this work was provided by Foundation for Science and Technology as a post-doctoral grant (SFRH/BPD/41047/2007) to M.J. Trindade, which is gratefully acknowledged. OSL dating was financed by the Ministerio Español de Ciencia (projects CGL2011-30141 e CGL2006-08996). The authors would like to thank two anonymous reviewers for their constructive suggestions that considerably improved the original manuscript.

REFERENCES

Adamiec, G., Aitken, M.J., 1998. Dose-rate conversion factors: update. Ancient TL, 16(2), 37-50.

Ahrens, L.H., Willis, J.P., Oosthuizen, C.O., 1967. Further observations on the composition of manganese nodules, with particular reference to some of the rarer elements. Geochim. Cosmochim. Acta, 31(11), 2169-2180.

Aitken, M.J., 1998. An introduction to optical dating: The dating of Quaternary sediments by the use of photon-stimulated luminescence. Oxford, Oxford University Press, 280pp.

Alonso, A., Pagés, J.L., 2000. El registro sedimentario del final del Cuaternario en el litoral noroeste de la Península Ibérica. Márgenes cantábrico y atlántico. Revista de la Sociedad Geológica de España, 23(1), 17-29.

Alonso, A., Pagés, J.L., 2007. Stratigraphy of Late Pleistocene coastal deposits in Northern Spain. Journal of Iberian Geology, 33(2), 207-220.

Anders, E., Grevesse, N., 1989. Abundances of the elements: Meteoritic and solar. Geochimica and Cosmochimica Acta, 53, 197-214.

Bailey, R.M., Arnold, L.J., 2006. Statistical modeling of single grain quartz De distributions and an assessment of procedures for estimating burial dose. Quaternary Science Reviews, 25(19-20), 2475-2502.

Beauvais, A., Roquin, C., 1996. Petrological differentiation patterns and geomorphic distribution of ferricretes in Central Africa. Geoderma, 73, 63-82.

Blanco Chao, R., Costa Casais, M., Martínez Cortizas, A., Pérez Alberti, A., Tranhaile, A.S., 2003. Evolution and inheritance of a rock coast: Western Galicia, Northwestern Spain. Earth Surf. Process. Landforms, 28, 757-775.

Braun, J-J., Pagel , M., Muller, J-P., Bilong, P., Michard, A., Guillet, B., 1990. Cerium anomalies in lateritic profiles. Geochimica and Cosmochimica Acta, 54, 781-795.

Burns, R.G., 1976. The uptake of cobalt into ferromanganese nodules, soils, and synthetic manganese (IV) oxides. Geochimica and Cosmochimica Acta, 40(1), 95-102.

Cao, X., Chen, Y., Wang, X., Deng, X., 2001. Effects of redox potential and pH value on the release of rare earth elements from soil. Chemosphere, 44(4), 655-661.

Coelho, M.R., Vidal-Torrado, P., 2000. Cério (Ce) em ferricretes nodulares desenvolvidos em solos da formação adamantina. Scientia Agricola, 57(2), 329-336.

Devoy, R.J.N., Delaney, C., Carter, R.W.G., Jennings, S.C., 1996. Coastal stratigraphies as indicators of environmental changes upon European coasts in the Late Holocene. Journal of Coastal Reserch, 12(3), 564-588.

Dias, M.I., Prudêncio, M.I., 2007. Neutron activation analysis of archaeological materials: an overview of the ITN NAA laboratory. Portugal, Archaeometry, 49(2), 383-393.

Dorronsoro, B., Aguilar, J., Dorronsoro-Díaz, C., Stoops, G., Sierra, M., Fernández, J., Dorronsoro-Fernández, C., 2006. Hidromorfía en suelos. Curso de Edafología. Universidad de Granada. Webpage: http://edafologia.ugr.es/hidro/concept.htm, accessed on June 11th, 2012.

Dowding, C.E., Fey, M.V., 2007. Morphological, chemical and mineralogical properties of sme manganese-rich oxisols derived from dolomite in Mpumalanga province, South Africa. Geoderma, 141(1-2), 23-33.

Flor, G., 1992. Tipología, catalogación y tendencias de los procesos de erosión/sedimentación de los campos dunares de la costa de Galicia (NW de España). Thalassas, 10, 9-39.

Galbraith, R.R., Laslett, G.M., 1993. Statistical models for mixed fission track ages. Radiation Measurements, 21(4), 459-470.

Galbraith, R.F., Roberts, R.G., Laslett, G.M., Yoshida, H., Olley, J.M., 1999. Optical dating of single and multiple grains of quartz from Jinmium rock shelter, northern Australia. Part I: experimental design and statistical models. Archaeometry, 41(2), 339-364.

Gallaher, R.N., Perkins, H.F., Radcliffe, D., 1973. Soil concretions: I. X-ray spectrograph and electron microprobe analyses. Soil Science Society of America Proceedings, 37(3), 465-469.

Gouveia, M.A., Prudêncio, M.I., 2000. New data on sixteen reference materials obtained by INAA. Journal of Radioanalytical and Nuclear Chemistry, 245(1), 105-108.

Granja, H., Carvalho, G., 1992. Dunes and Holocene deposits of the coastal zone of Portugal, north Mondego cape. In: Carter, R.W.G., Curtis, T.G.F., Sheethy-Skeffington, M.J. (eds.). Coastal Dunes: geomorphology, ecology and management for conservation. Galway (Ireland), Proceedings of the Third European Dune Congress, 43-50.

Gutiérrez Becker, L., López Cancelo, L., Vidal Romaní, J.R., Granja, M.E., 2004. Episodios eólicos durante el pleistoceno superior-Holoceno de la costa de Galicia: el caso de Punta Penaboa (A Coruña). In: Benito, G., Díez Herrero, A. (eds.). Contribuciones recientes sobre geomorfología. Sociedad Española de Geomorfología, CSIC-Centro de Ciencias Ambientales, Actas de la VIII Reunión Nacional de Geomorfología, 1, 253-261.

Hill, C.A., 1982. Origin of black deposits in caves. National Speleological Society Bulletin, 44(1), 15-19.

Koppi, A.J., Edis, R., Field, D.J., Geering, H.R., Klessa, D.A., Cockayne, J.H., 1996. Rare earth element trends and cerium-uranium-manganese associations in weathered rock from

Koongarra, Northern Territory, Australia. Geochimica and Cosmochimica Acta, 60(10), 1695-1707.

Korotev, R.L., 1996. A self-consistent compilation of elemental concentration data for 93 geochemical reference samples. Geostandards Newsletter, 20, 217-245.

López Cancelo, L., 2004. Cambios paleoambientales en el NW peninsular durante el Holoceno, determinados a partir del estudio de foraminíferos bentónicos. Universidad de A Coruña, Doctoral Thesis, 293pp.

López-González, F., Grandal-d'Anglade, Vidal-Romaní, J.R., 2006. Deciphering boné depositional sequences in caves through the study of manganese coatings. Journal of Archaeological Science, 33(5), 707-717.

Mackenzie, R.M., 1989. Manganese oxides and hydroxides. In: Dixon, J.B., Weed, S.B. (eds.). Mineral in soil environments. Madison, Soil Science Society of America, 439-461.

Marín Arroyo, A.B., Landete Ruíz, M.D., Vidal Bernabeu, G., Seva Román, R., González Morales, M.R., Straus, L.G., 2008. Archaeological implications of human-derived manganese coatings: a study of blackened bones in El Mirón Cave, Cantabrian Spain. Journal of Archaeological Science, 35(3), 801-813.

Moffett, J.W., 1994. The relationship between cerium and manganese oxidation in the marine environment. Limnology and Oceanography, 39(6), 1309-1318.

Mosquera Santé, M.J. 2000, Evolución post-glaciar del nível del mar en el NO de la península Ibérica: El caso del Golfo Ártabro. Universidad de A Coruña, Doctoral Thesis, 155pp.

Murray, J.W., Dillard, J.G., 1979. The oxidation of cobalt (II) adsorbed on manganese dioxide. Geochimica and Cosmochimica Acta, 43(5), 781-787.

Murray, A.S., Wintle, A.G., 2003. The single aliquot regenerative dose protocol: potential for improvements in reliability. Radiation Measurements, 37(4-5), 377-381.

Neaman, A., Martínez, C.E., Trolard, F., Bourrie, G., 2008. Trace element associations with Fe- and Mn-oxides in soil nodules: Comparison of selective dissolution with electron probe microanalysis. Applied Geochemistry., 23, 778-782.

Nesbitt, H.W., 1979. Mobility and fractionation of rare earth elements during weathering of a granodiorite. Nature, 279, 206-210.

Nieto, M.I., Vidal Romaní, J.R., 1989. Niveles marinos y depósitos continentales antiguos en el borde costero entre Cabo Prior y Cabo Prioriño (A Coruña, Galicia, España). Cadernos dp Laboratorio Xeolóxico de Laxe, 14, 67-78.

Palumbo, B., Bellanca, A., Neri, R., Roe, M.J., 2001. Trace element partitioning in Fe-Mn nodules from Sicilian soils, Italy. Chemical Geology, 173(4), 257-269.

Potter, R.M., Rossman, G.R., 1979. Mineralogy of manganese dendrites and coatings. Australian Journal of Soil Science, 19, 77-80.

Prescott, J.R., Hutton, J.T., 1995. Environmental dose rates and radioactive disequilibrium from some Australian luminescence dating sites. Quaternary Science Reviews, 14(4), 439-448.

Prudêncio, M.I., Sequeira Braga, M.A., Cabral, J.M.P., 1993. REE mobilization, fractionation and precipitation during weathering of basalts. Chemical Geology, 107(3-4), 251-254.

Roucoux, K.H., Tzedakis, P.C., de Abreu, L., Shackleton, N.J., 2006. Climate and vegetation changes 180.000 to 345.000 years ago recorded in a deep-sea core off Portugal. Earth Planetary Science Letters, 249, 307-325.

Roy, S., 2006. Sedimentary manganese mettalogenesis in response to the evolution of the Earth system. Earth-Science Reviews, 77, 273-305.

Santos Fidalgo, L., Bao Casal, R., Jalut, G., 1993. Estudio micropaleontológico de una turbera litoral holocena en la Ría de Ares (A Coruña). Cadernos do Laboratorio Xeolóxico de Laxe, 18, 175-188.

Sanz, A., García-González, M.T., Vizcayno, C., Rodríguez, R., 1996. Iron-manganese nodules in a semi-arid environment. Australian Journal of Soil Science, 34(5), 623-634.

Schultz, L.G., 1964. Quantitative interpretation of mineralogical composition X-ray and chemical data for the Pierre Shale. U.S. Geological Survey professional paper, 391-C, 1-31.

Sequeira Braga, M.A., Paquet, H., Begonha, A., 2002. Weathering of granites in a tenperate climate (NW Portugal): granitic saprolites and arenization. Catena, 49(1-2), 41-56.

Tan, W., Liu, F., Feng, X., Huang, Q., Li, X., 2005. Adsorption and redox reactions of heavy metals on Fe-Mn nodules from Chinese soils. Journal of Colloid and Interface Science, 284(2), 600-605.

Taunton, A.E., Welch, S.A., Banfield, J.F., 2000. Microbial controls on phosphate and lanthanide distributions during granite weathering and soil formation. Chemical Geology, 169(3-4), 371-382.

Taylor, R.M., 1968. The association of manganese and cobalt in soils – further observations. Australian Journal of Soil Science, 19(1), 77-80.

Thorez, J., 1976. Practical Identification of Clay Minerals. Belgium, Lelotte, 90pp.

Vidal Romaní, J.R., 1974. Sedimentos marinos antiguos en la costa de A Coruña. A Coruña, Spain. Depósito Laboratorio Xeolóxico de Laxe, trabajo inédito, 35pp.

Vidal Romaní, J.R., 1986. Estudio teórico sobre el origen de las características morfológicas de las pias (gnammas, vasque). Cadernos do Laboratorio Xeolóxico de Laxe: Revista de xeoloxía galega e do hercínico peninsular, 10, 133-168.

Vidal Romaní, J.R., Santos Fidalgo, L., López Cancelo, L., Mosquera Santé, M.J., Leira Campos, M., 2000. Storminess variation along the atlantic seaboard of Europe over the last 2000 years: Holocene strorminess from coastal barriers in North-West Spain, internal report Instituto Universitario de Xeoloxía "Isidro Parga Pondal", Universidade de a Coruña (Galicia, Spain).

Watanuki, T., Murray, A.S., Tsukamoto, S., 2005. Quartz and polymineral luminescence dating of Japanese loess over the last 0.6 Ma: comparison with an independent chronology. Earth Planetary Science Letters, 240(3-4), 774-789.

Wintle, A.G., Murray, A.S., 2006. A review of quartz optically stimulated luminescence characteristics and their relevance in single-aliquot regeneration dating protocols. Radiation Measurements, 41(4), 269-391.

Zhang, M., Karathanasis, A.D., 1997. Characterization of iron-manganese concretions in Kentucky alfisols with perched water tables. Clays Clay Miner., 45(3), 428-439.

Manuscript received November 2011;
revision accepted June 2012;
published Online January 2013.

ELECTRONIC APPENDIX

TABLE I | Results of X-ray diffraction analyses

	Sample	* Qtz	Pl	Kfs	Gib	Mica	Kln
GRANITIC ROCKS							
whole rock	PPB6	30	24	27	-	18	1
	PPB7	38	15	45	-	2	-
	PPB12	25	31	33	-	10	1
SLOPE DEPOSITS							
< 2 mm	PPB5	24	52	13	-	11	-
	PPB8.1	47	24	16	-	10	3
	PPB9	38	34	22	-	5	1
	PPB10	12	51	30	-	6	1
	PPB14.1	36	46	10	-	7	1
> 2 mm	PPB8.2	28	56	6	-	10	-
	PPB14.2	44	38	11	-	7	-
DUNE							
whole rock	PPB1	98	-	tr	-	-	2
	PPB2	99	tr	tr	-	-	-
	PPB3	96	tr	2	-	tr	1
	PPB4	96	tr	1	tr	1	1
< 63 µm	PPB1	43	-	7	2	10	38
	PPB2	27	8	15	1	10	39
	PPB3	26	4	5	1	39	25
	PPB4	27	5	14	2	30	22

* Qtz - quartz; Pl - plagioclase; Kfs - potassium feldspar; Gib - gibbsite; Kln - kaolinite; Mica - muscovite/illite; tr - traces.

TABLE II | Major (in wt% oxides) and trace (in µg/g) element composition of granitic rocks and slope deposits

	GRANITIC ROCKS			SLOPE DEPOSIT S (S.D.) (< 2 mm)					S.D. (> 2 mm)	
Sample	PPB6	PPB7	PPB12	PPB5	PPB8.1	PPB9	PPB10	PPB14.1	PPB8.2	PPB14.2
Na_2O	2.84	2.42	3.80	4.80	2.50	2.59	3.36	3.50	4.62	3.83
K_2O	4.46	4.34	5.78	3.84	3.44	3.29	3.49	3.47	3.60	3.69
MnO	0.038	0.031	0.032	0.027	0.039	0.035	0.033	0.032	0.031	0.023
Fe_2O_3T	1.66	2.50	1.78	0.666	2.05	2.88	2.18	1.85	0.782	0.653
Sc	4.40	6.02	4.56	0.124	3.88	4.91	4.30	4.34	0.475	0.386
Cr	6.96	11.8	6.85	2.42	16.9	22.3	18.1	17.6	3.32	2.61
Co	2.74	3.73	3.13	0.157	2.59	2.79	1.55	2.37	0.306	0.212
Zn	53.2	52.6	46.0	103	78.0	69.0	63.5	74.7	96.9	88.5
Ga	20.7	23.0	n.d.	21.9	27.9	34.0	20.1	23.8	n.d.	32.6
As	3.38	9.24	3.47	n.d.	9.70	13.4	8.07	7.93	2.17	3.40
Br	28.2	129	1.79	2.44	254	269	195	67.3	15.5	2.65
Rb	360	251	275	832	461	409	458	505	719	736
Zr	91.4	131	111	n.d.	128	112	132	91.5	11.3	33.5
Sb	*n.d.	0.104	0.183	n.d.	0.198	0.236	n.d.	0.197	n.d.	0.049
Cs	67.5	24.8	34.4	71.3	38.7	35.6	39.3	40.2	81.3	53.9
Ba	353	383	400	n.d.	151	245	201	129	n.d.	95.8
La	44.3	54.6	55.3	1.39	33.2	28.6	26.8	26	7.33	39.3
Ce	85.6	103	98.1	2.51	63.5	54.8	51.1	53.6	11.8	6.46
Nd	35.2	41.5	30.4	n.d.	26.3	22.3	20.3	22.6	4.91	1.41
Sm	5.64	6.89	7.16	0.154	4.24	3.82	3.27	4.16	0.868	0.455
Eu	0.727	0.792	1.07	0.066	0.534	0.526	0.438	0.555	0.135	0.131
Tb	0.309	0.526	0.599	0.220	0.451	0.38	0.354	0.378	0.095	0.033
Yb	2.16	1.90	1.80	0.346	1.56	1.40	1.23	1.48	0.491	0.458
Lu	0.207	0.256	0.188	n.d.	0.176	0.198	0.206	0.175	n.d.	0.038
Hf	3.95	5.48	4.56	0.798	4.12	4.53	4.20	3.71	1.59	1.37
Ta	10.5	2.00	1.75	3.11	5.34	2.93	2.78	3.56	2.94	2.47
W	2.14	n.d.	6.30	n.d.	1.69	2.45	2.69	n.d.	n.d.	n.d.
Th	30.2	41.2	31.8	0.445	20.5	18.3	12.2	15.6	3.10	1.91
U	8.18	14.0	10.7	0.917	4.66	4.30	2.96	6.63	1.42	0.928

* n.d. - not detected

TABLE III Major (in wt% oxides) and trace (in µg/g) element composition of host sand and nodular dune samples

DUNE	whole rock				host sand				dark nodular masses			
Sample	PPB1	PPB2	PPB3	PPB4	PPB1.1	PPB2.1	PPB3.1	PPB4.1	PPB1.2	PPB2.2	PPB3.2	PPB4.2
Na_2O	0.049	0.079	0.101	0.147	0.047	0.044	0.096	0.291	0.054	0.043	0.084	0.113
K_2O	0.485	0.413	0.674	0.751	0.397	0.370	0.542	0.901	0.407	0.338	0.542	0.648
MnO	0.022	0.012	0.015	0.107	0.012	0.006	0.007	0.019	0.990	0.411	0.262	0.617
Fe_2O_3T	0.478	0.394	0.514	0.668	0.498	0.457	0.523	0.688	0.926	0.655	0.895	0.831
Sc	1.68	1.35	1.93	3.87	1.72	1.60	1.97	3.20	6.63	3.74	4.29	10.9
Cr	9.7	6.97	8.50	12.1	10.5	9.89	11.0	12.4	8.31	6.35	10.8	8.16
Co	1.74	1.09	1.43	12.1	1.68	0.971	1.20	2.57	35.6	15.9	19.5	101
Zn	14.5	14.3	17.5	21.1	14.9	14.2	19.1	30.4	30.3	20.1	20.6	31.7
Ga	5.02	5.42	6.93	6.28	5.22	5.25	8.47	6.72	7.62	6.22	5.85	9.57
As	3.73	3.04	3.71	6.69	3.95	3.74	3.40	5.27	19.2	10.3	12.1	16.8
Br	14.8	14.1	16.1	23.2	15.4	17.8	17.1	22.5	18.7	16.1	23.1	40.5
Rb	49.2	55.6	78.2	94.8	48.1	39.1	77.2	148	45.2	40.4	61.8	69.1
Zr	35.1	32.1	61.0	91.1	34.8	43.8	41.8	74.4	130	107.1	239	224
Sb	0.199	0.189	0.180	0.300	0.187	0.116	0.159	0.226	1.33	0.587	0.720	0.960
Cs	7.42	7.52	9.37	10.5	7.82	6.19	10.9	15.1	8.16	6.94	8.99	8.45
Ba	37.4	34.3	67.5	116	38.1	51.0	37.0	63.6	1272	414	361	331
La	22.8	15.2	27.8	42.0	23.3	19.5	25.8	37.8	38.2	29.1	43.8	65.5
Ce	29.9	31.2	49.9	75.1	30.8	32.8	37.2	70.4	229	129	111	119
Nd	11.8	8.87	14.7	20.1	12.1	10.8	13.2	18.6	20.4	14.6	23.5	33.1
Sm	1.78	1.35	2.22	2.75	1.82	1.72	2.09	2.52	3.42	2.30	3.37	4.62
Eu	0.213	0.199	0.301	0.407	0.269	0.248	0.286	0.379	0.494	0.334	0.461	0.580
Tb	0.126	0.124	0.225	0.217	0.135	0.170	0.191	0.204	0.333	0.197	0.251	0.339
Yb	0.349	0.279	0.645	0.589	0.358	0.399	0.485	0.512	0.851	0.506	0.900	0.652
Lu	0.040	0.036	0.070	0.050	0.044	0.051	0.054	0.047	0.071	0.080	0.070	0.056
Hf	1.29	1.15	2.08	3.02	1.37	1.32	1.80	2.81	3.74	3.21	6.36	7.02
Ta	0.665	0.575	0.839	1.030	0.676	0.634	0.99	1.15	0.848	0.618	1.13	0.984
W	0.461	0.275	0.411	0.523	0.483	0.460	0.432	0.540	0.792	0.592	0.445	0.597
Th	12.0	10.2	16.8	22.3	12.8	12.3	14.6	18.8	58.4	36.9	46.5	54.3
U	2.24	1.98	2.63	2.70	2.33	2.49	2.68	2.76	4.28	2.88	2.97	5.37

TABLE IV Elemental enrichment factors (EF) in the nodular masses relative to the host sand for the four dune samples and their average

Sample	EF_{PPB1}	EF_{PPB2}	EF_{PPB3}	EF_{PPB4}	$EF_{average}$
Mn	83	70	35	32	55
Co	21	16	16	39	23
Ba	33	8.1	9.8	5.2	14
Sb	7.1	5.1	4.5	4.3	5.2
Ce	7.4	3.9	3.0	1.7	4.0
Zr	3.7	2.4	5.7	3.0	3.7
As	4.9	2.8	3.6	3.2	3.6
Th	4.6	3.0	3.2	2.9	3.4
Sc	3.9	2.3	2.2	3.4	2.9
Hf	2.7	2.4	3.5	2.5	2.8
Nd	1.7	1.4	1.8	1.8	1.7
Sm	1.9	1.3	1.6	1.8	1.7
Tb	2.5	1.2	1.3	1.7	1.7
Yb	2.4	1.3	1.9	1.3	1.7
La	1.6	1.5	1.7	1.7	1.6
Eu	1.8	1.3	1.6	1.5	1.6
Lu	1.6	1.6	1.3	1.2	1.4
Fe	1.9	1.4	1.7	1.2	1.6
U	1.8	1.2	1.1	2.0	1.5
Zn	2.0	1.4	1.1	1.0	1.4
Br	1.2	0.9	1.4	1.8	1.3
W	1.6	1.3	1.0	1.1	1.3
Ga	1.5	1.2	0.7	1.4	1.2
Ta	1.3	1.0	1.1	0.9	1.1
K	1.0	0.9	1.0	0.7	0.9
Na	1.2	1.0	0.9	0.4	0.9
Cs	1.0	1.1	0.8	0.6	0.9
Rb	0.9	1.0	0.8	0.5	0.8
Cr	0.8	0.6	1.0	0.7	0.8

TABLE V | REEs parameters for the host sand and dark nodular dune samples

DUNE	Sample	*(La/Yb)n	Eu anomaly	Ce anomaly
host sand	PPB1. 1	44.9	0.580	0.795
	PPB2. 1	33.7	0.514	0.994
	PPB3. 1	36.7	0.501	0.872
	PPB4. 1	50.9	0.573	1.14
nodular masses	PPB1. 2	31.0	0.517	3.58
	PPB2.2	39.7	0.543	2.71
	PPB3.2	33.6	0.536	1.51
	PPB4.2	69.3	0.494	1.10

* normalized lanthanum-ytterbium ratio

TABLE VI | Results on dosimetry and other measurements used for luminescence dating of two dune samples from Penaboa Aeolian deposit. Conversion factors of radionuclide activities to determine the annual dose were taken from Adamiec and Aitken (1998); W.C. is the water weight/weight of dried sample ratio, being the attenuation factors used for the calculation of water influence in annual dose, those of Zimmerman (1971); The contribution of cosmic rays in annual dose is included in annual dose calculation in accordance to Prescott and Hutton (1995); N is the number of aliquots used to obtain De; De is the equivalent dose determined considering the central age (arithmetic mean coincident with weighted mean and CAM)

Sample	05/009-Penaboa 1	05/010-Penaboa 2
Procedure	OSL-SAR	OSL-SAR
^{238}U (Bq kg $^{-1}$)	2.9 ± 9.4	32 ± 5
^{226}Ra (Bq kg $^{-1}$)	9.8 ± 1.5	33.2 ± 0.61
^{232}Th (Bq kg $^{-1}$)	21.9 ± 1.4	36.5 ± 0.6
^{40}K (Bq kg $^{-1}$)	118 ± 28	149 ± 6.0
Dose Beta (Gy ka^{-1})	0.44 ± 0.07	0.59 ± 0.03
Dose Gamma (Gy ka^{-1})	0.63 ± 0.03	0.56 ± 0.02
W.C. (wt %)	2.7	8.7
Total annual dose	1.14 ± 0.07	1.22 ± 0.04
D_e (Gy)	332.5 ± 54	370.0 ± 59.0
N	16	18
Age (ka)	292 ± 51	304 ± 49